Available online at www.sciencedirect.com

SCIENCE DIRECT

Solid State Ionics 176 (2005) 25–31

SOLID STATE IONICS

www.elsevier.com/locate/ssi

Functionally graded cathodes fabricated by sol-gel/slurry coating for honeycomb SOFCs

Shaowu Zha, Yuelan Zhang, Meilin Liu*

School of Materials Science and Engineering, Georgia Institute of Technology, Atlanta, GA 30332-0245, United States

Received 18 February 2004; received in revised form 15 July 2004; accepted 20 July 2004

Abstract

Functionally graded cathodes for honeycomb solid oxide fuel cells are prepared using sol-gel/slurry coating techniques. The compositions of the cathodes are gradually changed from a material that is active for oxygen reduction and more compatible with the electrolyte (e.g., LSM for YSZ) to another material that is more conductive for current collection. The microstructure and electrochemical properties of the electrodes are systematically characterized using electron microscopy and electrochemical impedance spectroscopy. The cathodic interfacial polarization resistances for a graded cathode fired at 900 °C are 0.21 and 0.10 Ω cm^2 at 700 and 800 °C, respectively. The impedance spectra indicate that at least two separate processes contribute to the overall polarization resistances. The effects of cathode fabrication temperature and oxygen partial pressure on the high- and low-frequency impedance responses are studied in detail.

Keywords: Functionally graded cathodes; Honeycomb SOFCs; Sol-gel; Slurry coating; Impedance spectroscopy

1. Introduction

For a traditional solid oxide fuel cell (SOFC) with (La,Sr)MnO_3 (LSM) as the cathode and YSZ as the electrolyte, the performance is often limited by the oxygen reduction processes at the cathode [1–3]. This is especially true for SOFCs based on thin-electrolyte and operated on H_2 fuel, where the resistances of the electrolyte and anode are relatively small [4–6]. In order to improve SOFC performance, both composition and structure of the LSM/YSZ interface as well as the cathode must be optimized to provide a higher density of active sites such as triple phase boundaries (TPBs) for electrode reactions. Towards this end, several composite electrodes are developed to replace the LSM electrodes such as LSM–YSZ, LSM–GDC (i.e. gadolinium-doped ceria), and LSCF [i.e. (La,Sr)(Co,Fe)O_3]–GDC, where additional TPBs within the electrode can contribute to the electrode reactions [7–12].

The interfacial polarization resistance of an LSM–GDC composite is about half that of an LSM–YSZ composite cathode on a YSZ electrolyte when they have similar microstructure due probably to the fact that GDC has much higher ionic conductivity than YSZ at reduced temperatures [10]. However, the sheet resistance of a composite LSM cathode is relatively high, resulting in large ohmic drop due to current collection. The advantages of adding a layer of current collector are demonstrated by the addition of an LSM layer over the LSM–YSZ composite layer [13]. (La,Sr)CoO_3 (LSC) and LSCF have been identified as cathode materials that offer improved electrical conductivity, for example, 320 S cm^{-1} for LSCF at 700 °C. However, LSCF has a higher thermal expansion coefficient (TEC, 15.3×10^{-6} K^{-1}) and LSC even much higher TEC (23×10^{-6} K^{-1}) than YSZ (10.8×10^{-6} K^{-1}), GDC (12.5×10^{-6} K^{-1}), and LSM (12.0×10^{-6} K^{-1}) [14–17]. It has also been shown that LSC and LSCF readily react with YSZ to form $La_2Zr_2O_7$ and $SrZrO_3$ resistive compounds

* Corresponding author.
E-mail address: meilin.liu@mse.gatech.edu (M. Liu).

0167-2738/$ - see front matter © 2004 Elsevier B.V. All rights reserved.
doi:10.1016/j.ssi.2004.07.010

under fabrication conditions, resulting in poor electrode performance [18,19]. To avoid these undesirable reactions at the interface and sharp discontinuities in TECs, which could result in delamination during thermal cycling, cathodes graded in composition were developed with their electronic conducting phase gradually changed from LSM to LSC or LSCF [20–23].

Recently, we have been developing some unique fuel cell structures named as monolithic and hybrid honeycomb fuel cells [24]. In a monolithic honeycomb fuel cell, for example, ceramic honeycomb is fabricated by extruding YSZ powder paste through a complex die followed by heat treatment to sinter cell walls to full density. Then the fuel cell will be constructed by depositing anodes and cathodes from slurries onto the walls of the YSZ honeycomb. Fig. 1 shows the schematic diagram of this fuel cell. For planar operation, a manifold is needed at each end of the 4×4 cell array. These two manifolds create a hermetic system to allow passage of fuel through anode planes of the cells while air is passed through the adjacent cathode layers. While the concept of functionally graded electrode has been demonstrated by other techniques such as combustion CVD [25], the application of this functionally graded electrode to honeycomb fuel cell poses additional challenges due to the unique cell structures. Thus, one of the most important tasks is to develop appropriate electroding process and special electrode structure, which can meet the fuel cell demands such as an excellent electrode performance.

Here, we report our recent results on fabrication and characterization of LSM–LSCF–GDC based functionally graded cathodes for honeycomb fuel cells using sol-gel and slurry coating techniques. The composition was gradually changed from a catalytically active layer to a current collection layer.

2. Experimental

2.1. Preparation of GDC sol

The sol of $Ce_{0.9}Gd_{0.1}O_{1.95}$ was prepared from $(NH_4)_2Ce(NO_3)_6 \cdot 6H_2O$ and $Gd(NO_3)_3 \cdot 6H_2O$ (Aldrich, 99.9%). Stoichiometric amounts of the nitrates were mixed in distilled water and dripped into an ammonia solution (pH>11) under vigorous stirring to form pale yellow hydroxide precipitate, which was then washed and filtered five times using distilled water to remove NH_4NO_3. The resulted hydroxide suspension was then peptized with dilute nitric acid (1 mol/l) to pH 3.5, followed by keeping it at 85 °C for 10 h to form a clear GDC sol.

2.2. Preparation of slurry

$La_{0.72}Sr_{0.18}MnO_3$ and $La_{0.6}Sr_{0.4}Co_{0.2}Fe_{0.8}O_3$ powders were synthesized via a glycine-nitrate combustion process (GNP) [26,27] with precursors of $La(NO_3)_3$, $Sr(NO_3)_2$, $Mn(NO_3)_2$/$Co(NO_3)_2$, and $Fe(NO_3)_3$ (Aldrich, 99.9%) and glycine (Alfa AeSAR, 99%). The mole ratio of nitrate ion to glycine was kept at 2:1 to get a complete combustion. The as-prepared powders were fired at 850 °C for 4 h to form the perovskite phase as confirmed by X-ray diffraction.

The fired powders were subsequently dispersed into the GDC sol together with polyvinyl alcohol (PVA, 0.8 wt.% of the total sol–powder mixture). The oxide powders derived from the GNP to the GDC sol were set at the values to

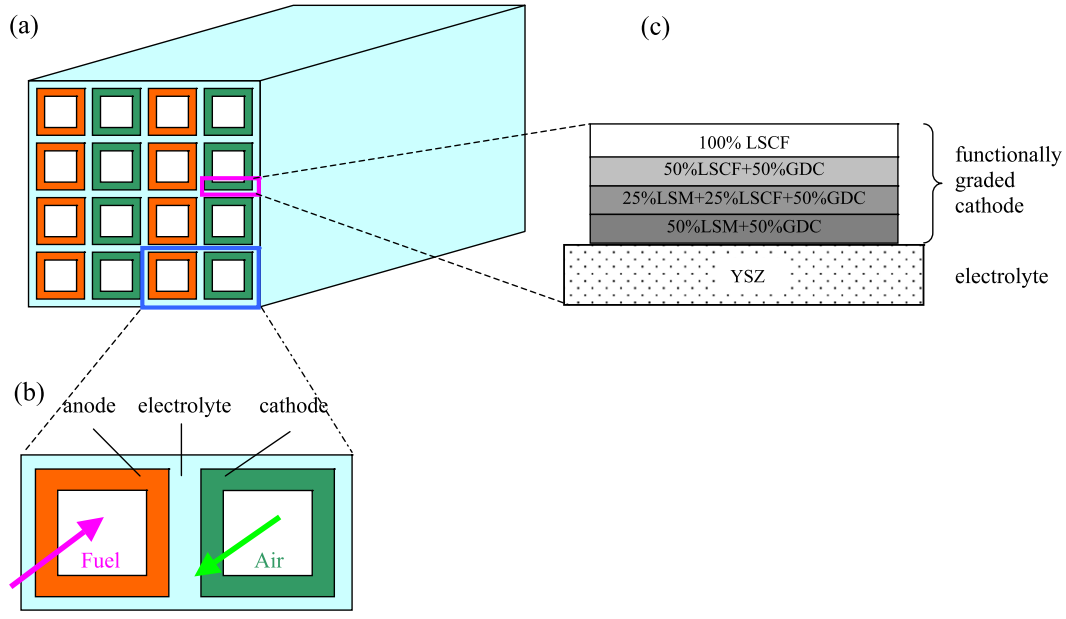

Fig. 1. Schematic illustration of (a) a honeycomb fuel cell, (b) a single cell, and (c) four-layered graded cathode fabricated in this study.

produce weight ratios of (a) LSM/GDC=50:50, (b) LSM/LSCF/GDC=25:25:50, and (c) LSCF/GDC=50:50. The mixtures were ball-milled to form sol-particle slurries. The suspensions were then heated at 80 °C to vaporize water until the GDC concentration was about 10 wt.% followed by ball-milling for 24 h.

2.3. Fabrication of functionally graded cathodes on honeycomb cells

Schematically shown in Fig. 1(a) is a cross-sectional view of a honeycomb cell, which was fabricated by extrusion of YSZ powder and followed by sintering in air at 1400 °C for 4 h [24]. The fired honeycomb has 16 channels (4×4) with wall thickness of 150 μm and length of 3 cm and a distance between adjacent walls of 1.6 mm. The sol-particle suspensions were dip-coated into the inner channels of YSZ honeycombs. Schematically shown in Fig. 1(c) is a cathode composed of GDC, LSM, and LSCF, with LSM content gradually decreased and LSCF content gradually increased in the direction away from the YSZ electrolyte–electrode interface. Each coated electrode layer was dried at 70 °C for 6 h and fired at 800 °C for 2 h before a subsequent layer was applied. The heating and cooling rates were 1 and 3 °C/min, respectively. Each of the four individual compositions was coated twice. Repeating the coating–drying–firing procedure eight times resulted in a graded layer of about 10-μm thickness. Finally, the graded

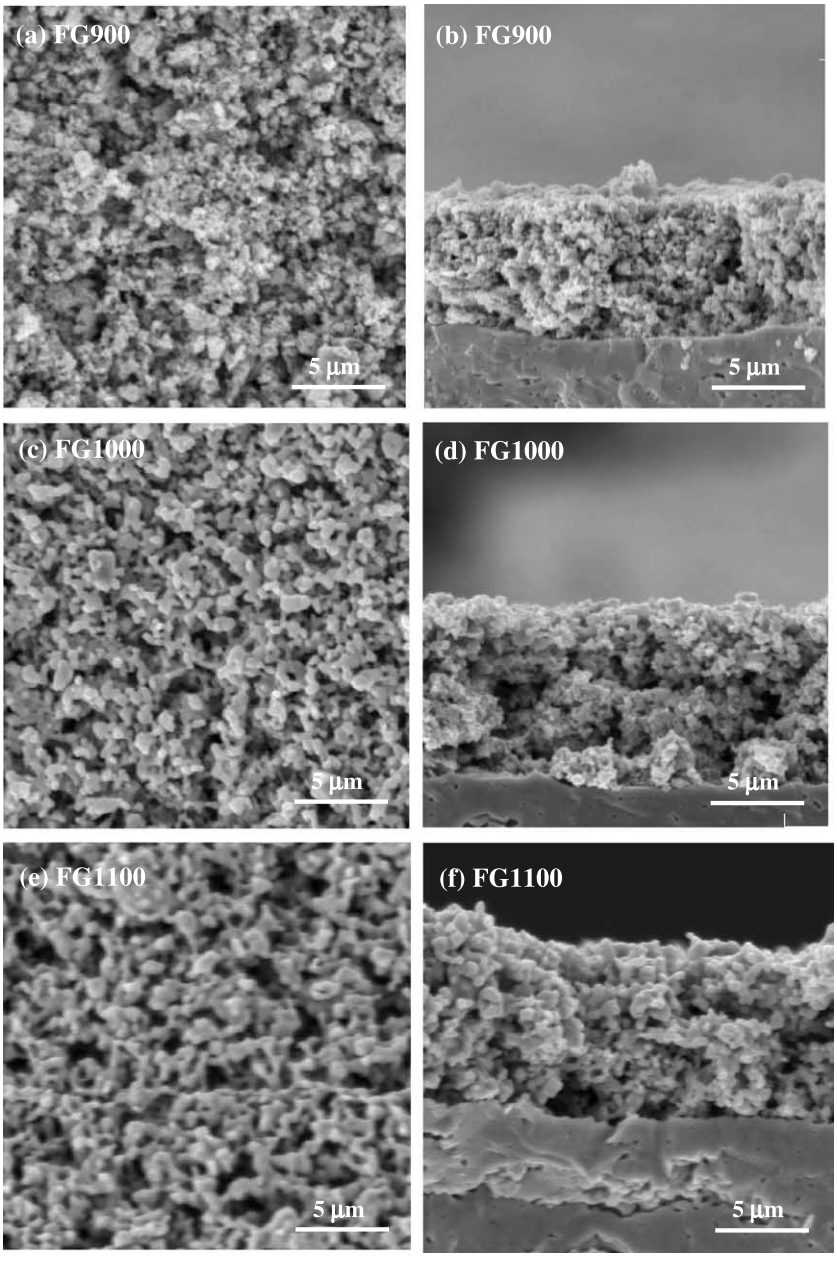

Fig. 2. Surface (left) and cross-sectional (right) views of functionally graded cathodes fired at 900, 1000, and 1100 °C, separately.

cathodes were fired at a temperature between 900 and 1100 °C for 2 h to attain functional electrode structures. The samples are labeled using the final firing temperature. For instance, FG900 refers to the sample that was fired at 900 °C for 2 h.

2.4. Characterization of microstructure and electrochemical performance

Scanning electron microscopy (SEM, Hitachi S-800) was used to observe the morphology and microstructure of electrodes fired at different temperatures. Two adjacent channels of the honeycomb cell were used for electrochemical measurement. Impedance spectra of these symmetrical cells were measured in air using an EG&G impedance system consisting of a lock-in amplifier (model 5210) and an EG&G potentiostat/galvanostat (model 273 A). Silver wires were attached to the electrodes with a silver paste, and a thermocouple was positioned close to the sample to provide an accurate measurement of the sample temperature, usually decreasing from 800 to 500 °C in 50 °C interval. Spectra were obtained in a frequency range typically from 100 kHz to 1 mHz with an applied ac voltage amplitude of 20 mV. All data were taken 30 min after the desired temperature was reached. In addition to impedance data collected in air, the impedances of two samples (FG900 and FG1050) were also measured in 1% and 0.1% O_2 (balanced with Ar).

3. Results and discussion

3.1. Microstructure of graded cathodes

Shown in Fig. 2 are surface and cross-sectional views (SEM photographs) of the functionally graded cathodes FG900, FG1000, and FG1100, respectively. These SEM micrographs reveal that the firing temperature has a strong influence on the microstructure. As expected, the cathode microstructure became coarser as the final firing temperature was increased from 900 to 1100 °C. All cathodes appear to have uniform microstructure and continuous contact with the dense electrolyte honeycomb walls. Also, no distinguishable variation in microstructures is observed across the four individual layers of different composition because of gradual change in composition.

3.2. Interfacial polarization resistances

Fig. 3(a) shows typical impedance spectra for a symmetrical cell with GDC–LSM–LSCF cathodes measured in air at 500–800 °C. At each temperature, two distinct processes appear to dominate the impedance response, one at high frequencies (HF) and one at low frequencies (LF) with a characteristic frequency at about 1 kHz and 0.2 Hz, respectively. While the high-frequency process dominated at lower temperatures and the corresponding impedance decreased rapidly with increasing temperature, the low-frequency process dominated at higher temperatures, as shown in Fig. 3(b). It is widely recognized that many interfacial processes may contribute to the interfacial impedance, including charge transfer and mass transport [3]. The main contribution to the ohmic polarization is due to the electrolyte, whose value (R_b) can be determined from the intercept of the impedance loop with the real axis at high frequencies.

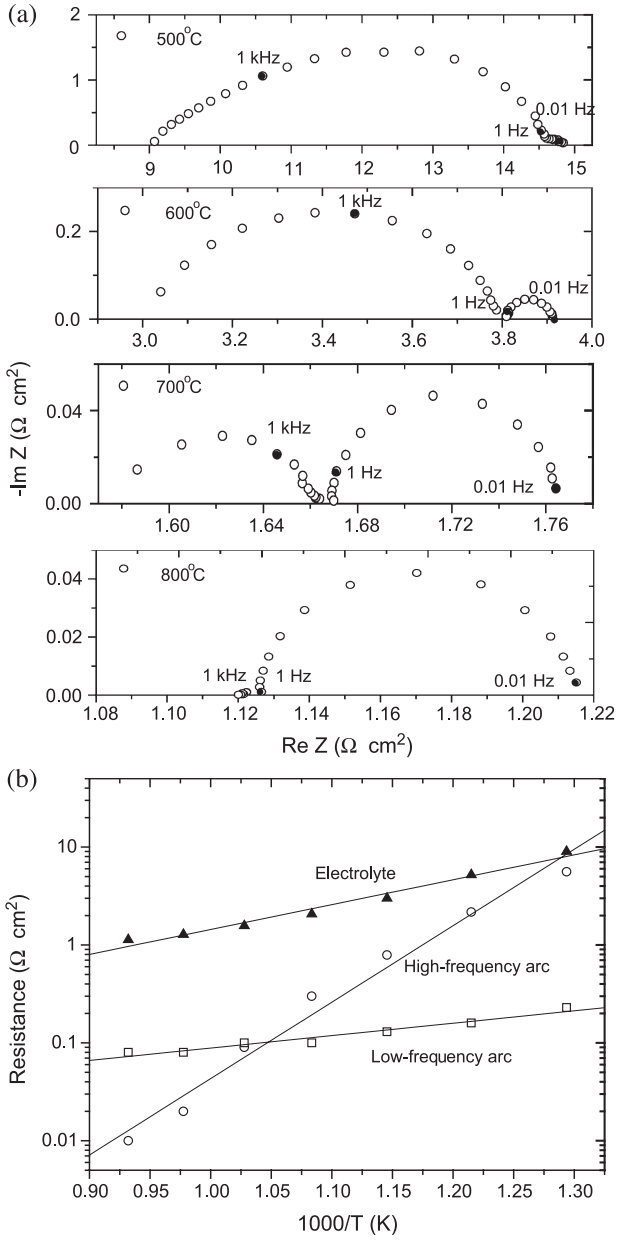

Fig. 3. (a) Typical impedance spectra and (b) dependence of the different resistances on temperature measured in air for the cathode FG900.

The total polarization resistances of the functionally graded cathode can be readily obtained from the difference between the high-frequency and low-frequency intercepts of impedance loop with the real axis. In the

two-electrode configuration, the total interfacial polarization impedance corresponds to the sum of all resistances arising from the electrochemical processes occurring at both electrode–electrolyte interfaces. For an ideal symmetrical cell under open circuit conditions (OC), as in the honeycomb structure, the contribution of each electrode is about half of the total impedance. Thus, if the total polarization resistance of the symmetrical cell under OCV is denoted as $2R_p$, the polarization resistance of each electrode–electrolyte interface would be R_p, which is used to characterize the performance of functionally graded electrodes.

Shown in Fig. 4 is the dependence of polarization resistance on the firing temperature of graded cathodes. The activation energy, determined from the slope, is also shown here. The values of activation energy vary from 1.03 to 1.14 eV, similar to those reported by Hart et al. [20] but much lower than those reported by others [11,12,23]. The benefits of using a lower firing temperature are clearly illustrated here. The polarization resistance measured at 800 °C is 0.43 Ω cm^2 for a cathode FG1100 and decreases to only 0.10 Ω cm^2 for a cathode FG900. The decrease in cathodic performance at high firing temperature is in accordance with a decreased length of the TPB in a coarse structure due to the larger average grain size developed during high-temperature firing. Reducing the cathode firing temperature lower than 900 °C may be possible to further decrease the polarization resistance. However, from practical point of view, the resulted finer microstructure as-prepared at lower temperatures will be readily coarsened which can cause rapid performance degradation in a long-term operation.

Fig. 5 compares the polarization resistances of FG900 with composite cathode (GDC–LSM) and functionally graded cathodes prepared using other methods [10,21,23]. Clearly, the GDC–LSM–LSCF functionally graded cathodes fabricated by sol-gel/slurry coating technique display much

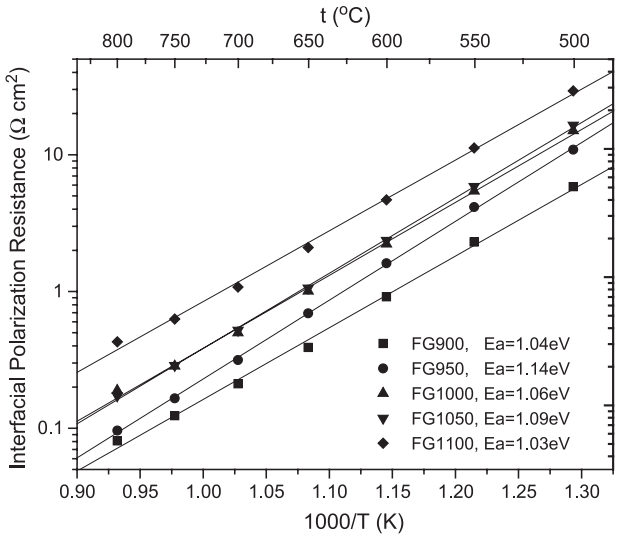

Fig. 4. Arrhenius plots of interfacial polarization resistances of the graded cathodes fired at 900–1100 °C.

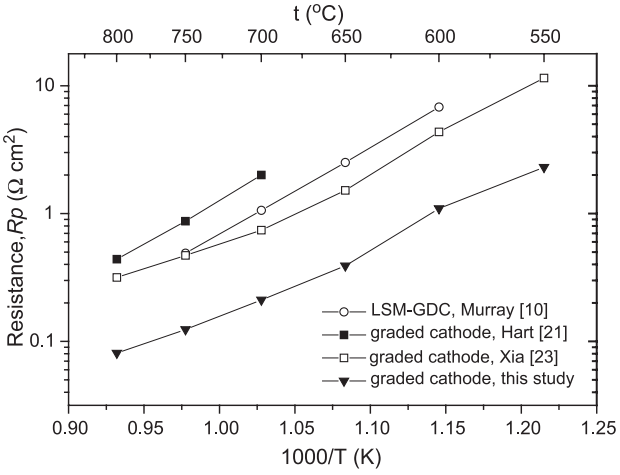

Fig. 5. Comparisons of interfacial polarization resistances of one composite and various graded cathodes derived from different fabrication processes.

smaller electrode polarization resistances than those prepared by other techniques. At 700 °C, for example, the cathodic polarization resistance for FG900 is only 0.21 Ω cm^2, compared to 0.74 Ω cm^2 for another graded cathode [23] and 2.0 Ω cm^2 for a GDC–LSM composite [10],

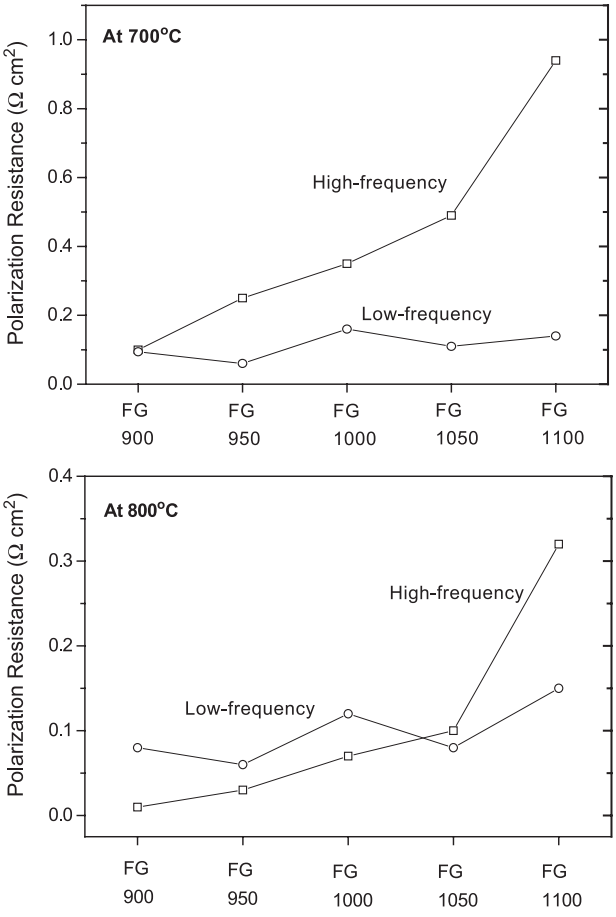

Fig. 6. The dependence of interfacial polarization resistance on fabrication temperature for cathodes FG900–FG1100 at 700 °C (upper panel) and 800 °C (lower panel), respectively.

implying about four times to one order of magnitude improvement. The superior electrochemical performance of the functionally graded cathode FG900 is ascribed to the following reasons. It is believed that composite layer of LSM–GDC, comprised by a contiguous electronically conducting electrode material and ionically conducting phase, can extend electrochemical reactions to occur within the electrode [12]. The addition of smaller GDC by sol-gel and annealing process will result in suppressing the growth of LSM grains and therefore sustaining the porosity and forming more contact points, creating a greater density of reaction sites within the cathode. Also, because of the physical and chemical compatibility of the cathode layers fabricated in graded compositions from LSM–GDC to pure LSCF, the adhesion of the electrode to the electrolyte and the contact between adjacent layers were significantly improved, which will reduce the risk of cathode structural defects and thus improve the cathode electrochemical performance.

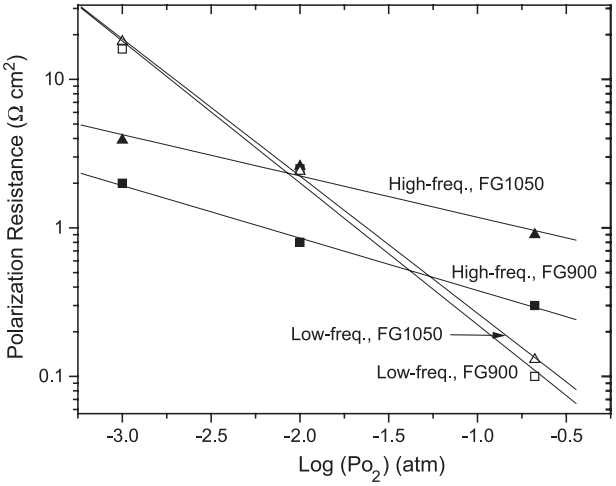

Fig. 8. Effect of oxygen partial pressure on the high- and low-frequency contributions to the polarization resistance for graded cathodes FG900 and FG1050 at 650 °C.

3.3. Factors influencing cathodic polarizations

3.3.1. Firing temperature

Shown in Fig. 6 are the resistances measured at 700 and 800 °C for five graded cathodes fired at different temperatures, FG900–FG1100, respectively. The high-frequency part of the EIS arcs increases rapidly with the firing temperature. The corresponding polarization measured at 700 °C decreased dramatically from 0.95 Ω cm^2 for FG1100 to 0.10 Ω cm^2 for FG900, whose cathode firing temperature was decreased from 1100 to 900 °C. Meanwhile, the characteristic frequency was increased as the final firing temperature decreasing. The large change in polarization resistance is due to the structural change in the cathodes arising from lower sintering temperature, such as an increase in contact area between the ionic and electronic components.

On the other hand, the low-frequency element of the EIS arcs is largely unaffected by the sintering temperature. The corresponding polarization resistance kept almost stable at

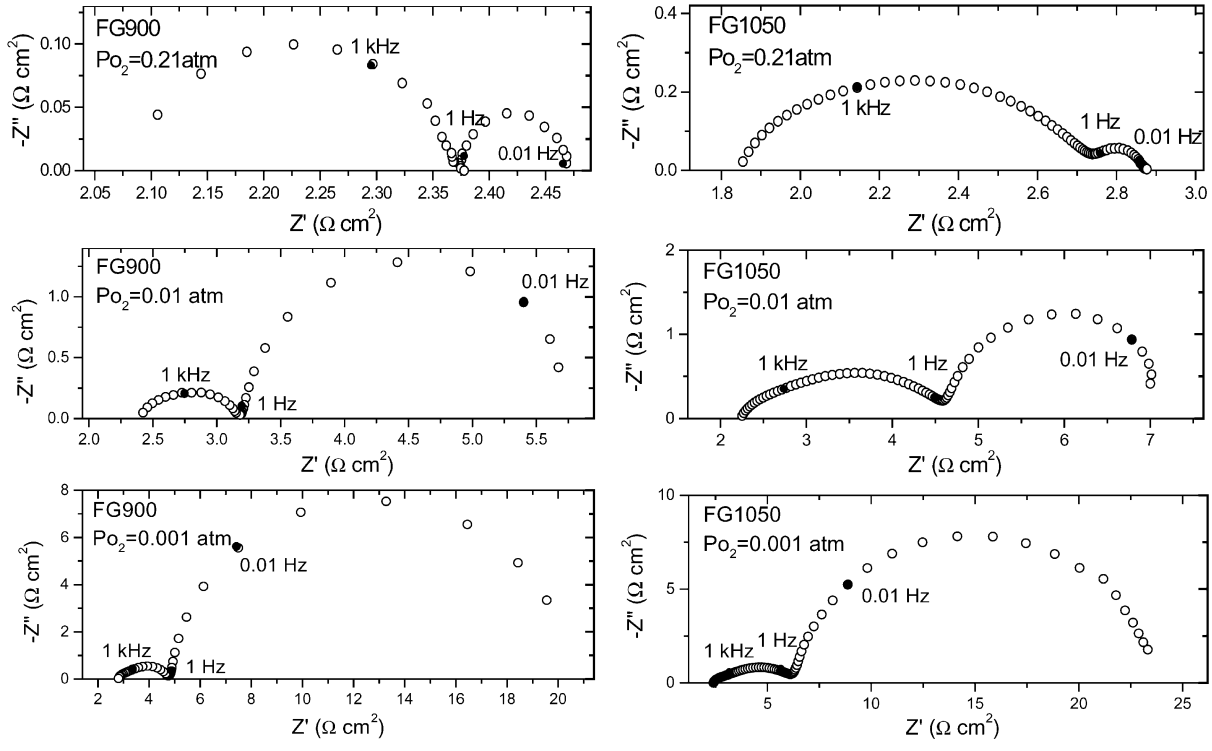

Fig. 7. Impedance spectra of the graded cathodes FG900 and FG1050 under various oxygen partial pressures at 650 °C.

the value of about 0.1 Ω cm^2 for samples FG900–FG1100. The characteristic frequency is 0.2 Hz for all low-frequency arcs. It is very interesting that the corresponding resistances at low-frequency process also showed little dependence on temperature in the range 500–800 °C, as shown in Fig. 3.

3.3.2. Oxygen partial pressure

The oxygen partial pressure dependence measured at 650 °C is plotted in Fig. 7 for graded cathodes FG900 and FG1050. When the graded samples were measured in oxygen-depleted synthetic air, the EIS response was clearly extended in the low-frequency region, while the high-frequency region showed little change for both samples.

On decreasing the oxygen content from 21% to 1% and 0.1%, sample FG900 showed a small increase in high-frequency related polarization from 0.3 to 0.8 and 2.0 Ω cm^2, but a large increase in low-frequency related polarization from 0.1 to 2.5 and 16 Ω cm^2, respectively. The characteristic frequency corresponding to the low-frequency process was also sensitive to changes in the oxygen partial pressure. It decreased from 0.2 to 0.025 and 0.004 Hz when the oxygen content decreased from 21% to 1% and 0.1%, respectively, for both samples FG900 and FG1050.

Fig. 8 illustrates the effect of P_{O_2} on the low- and high-frequency contribution to the overall polarization resistance of samples FG900 and FG1050 at 650 °C. The slope of the high-frequency element shows $P_{O_2}^{-0.35}$ and $P_{O_2}^{-0.28}$ dependence for FG900 and FG1050. In contrast, the low-frequency element displays a significant dependence of $P_{O_2}^{-0.95}$ and $P_{O_2}^{-0.93}$ for FG900 and FG1050, respectively. This is quite consistent with the $P_{O_2}^{-1}$ dependence expected for gas diffusion [28].

4. Conclusions

We have successfully fabricated functionally graded cathodes in LSM–LSCF–GDC composition system by a sol-gel/slurry coating process. The graded cathodes fired at 900 °C show relatively low polarization resistance at intermediate temperatures. Impedance analysis indicated that the overall polarization resistance of the graded electrodes on YSZ might be resulted from at least two separate processes. The high-frequency related polarization resistance was increased dramatically with the increasing sintering temperature of the cathodes. On the other hand, the low-frequency related polarization resistance displayed a significant dependence on the oxygen partial pressure.

Acknowledgements

The authors wish to gratefully acknowledge Kevin Hurysz, J. K. Lee, and Joe Cochran for fabrication of the YSZ honeycombs. This work was supported by Department of Energy (Grant DE-FG26-01NT41274) and by the DARPA/DSO Palm Power program funded through ARMY/ARO (Grant DAAD19-01-1-0649).

References

[1] M.J.L. Ostergard, C. Clausen, C. Bagger, M. Mogensen, Electrochem. Acta 40 (1995) 1971.
[2] J. Van Herle, A.J. McEvoy, K.R. Thampi, Electrochem. Acta 41 (1996) 1447.
[3] C.W. Tanner, K.Z. Fung, A.V. Virkar, J. Electrochem. Soc. 144 (1997) 21.
[4] J.P.P. Huijsmans, F.P.F. van Berkel, G.M. Christie, J. Power Sources 71 (1998) 107.
[5] J. Will, A. Mitterdorfer, C. Kleinlogel, D. Perednis, L.J. Gauckler, Solid State Ionics 131 (2000) 79.
[6] T. Tsai, S.A. Barnett, Solid State Ionics 93 (1997) 207.
[7] M. Juhl, S. Primdahl, C. Manon, M. Mogensen, J. Power Sources 61 (1996) 173.
[8] E.P. Murray, T. Tsai, S.A. Barnett, Solid State Ionics 110 (1998) 235.
[9] M. Sahibzada, B.C.H. Steele, K. Zheng, R.A. Rudkin, I.S. Metcalfe, Catal. Today 38 (1997) 459.
[10] E.P. Murray, S.A. Barnett, Solid State Ionics 143 (2001) 265.
[11] V. Dusastre, J.A. Kilner, Solid State Ionics 126 (1999) 163.
[12] E.P. Murray, M.J. Sever, S.A. Barnett, Solid State Ionics 148 (2002) 27.
[13] M.J. Jorgensen, S. Primdahl, C. Bagger, M. Mogensen, Solid State Ionics 139 (2001) 1.
[14] L.-W. Tai, M.M. Nasrallah, H.U. Anderson, D.M. Sparlin, S.R. Schlin, Solid State Ionics 76 (1995) 273.
[15] S.P.S. Badwal, A.E. Hughes, in: F. Grosz, et al. (Ed.), Proceedings of the Second International Symposium on Solid Oxide Fuel Cells, Luxembourg, 1991, p. 445.
[16] B.C.H. Steele, Solid State Ionics 75 (1995) 157.
[17] H. Michibata, H. Tenmei, T. Namikawa, Y. Yamazaki, in: S.C. Singhal (Ed.), Proceedings of the First International Symposium on Solid Oxide Fuel Cells, Electrochemical Society, Pennington, NJ, 1989, p. 188.
[18] H.Y. Tu, Y. Takeda, N. Imanishi, O. Yamamoto, Solid State Ionics 117 (1999) 277.
[19] R. Doshi, V.L. Richards, J.D. Carter, X. Wang, M. Krumpelt, J. Electrochem. Soc. 146 (1999) 1273.
[20] N.T. Hart, N.P. Brandon, M.J. Day, J.E. Shemilt, J. Mater. Sci. 36 (2001) 1077.
[21] N.T. Hart, N.P. Brandon, M.J. Day, N. Lapena-Rey, J. Power Sources 106 (2002) 42.
[22] P. Holtappels, C. Bagger, J. Eur. Ceram. Soc. 22 (2002) 41.
[23] C. Xia, W. Rauch, W. Wellborn, M. Liu, Electrochem. Solid-State Lett. 5 (2002) A217.
[24] C. Xia, W. Rauch, M. Liu, J. Cochran, J. Lee, M. Liu, Proceeding of the First International Conference on Materials Processing for Properties and Performance (MP3), Singapore, 2002.
[25] Y. Liu, S. Zha, M. Liu, Adv. Mater. 16 (2004) 256.
[26] L.A. Chick, L.R. Pedersen, G.D. Maupin, J.L. Bates, L.E. Thomas, G.J. Exarhos, Mater. Lett. 10 (1990) 6.
[27] S. Zha, W. Rauch, M. Liu, Solid State Ionics 166 (2004) 241.
[28] S.P.S. Badwal, J. Electroanal. Chem. 161 (1984) 75.